Absence and presence of Dirac electrons in silicene on substrates

Zhi-Xin Guo,* Shinnosuke Furuya, Jun-ichi Iwata, and Atsushi Oshiyama
Department of Applied Physics, The University of Tokyo, Tokyo 113-8656, Japan
(Received 14 November 2012; revised manuscript received 24 April 2013; published 27 June 2013)

We report on the total-energy electronic-structure calculations on the basis of the density-functional theory that clarify atomic and electronic structures of the silicene on the Ag(111), the hexagonal BN, and the hydrogen-processed Si(111) surfaces. On the Ag(111) surfaces which are most commonly used as substrates for the silicene in current experiments, we find several stable and metastable structures with the 4×4, $\sqrt{13} \times \sqrt{13}$, and $2\sqrt{3} \times 2\sqrt{3}$ periodicities with respect to the 1×1 Ag(111) lateral cell within the total-energy difference of 70 meV per Si atom. Those stable structures show the excellent agreement with the scanning tunneling microscopy measurement in their structural characteristics. The metastable structures with comparable total energies await experimental observations. In all the stable and metastable structures, the silicene is buckled substantially so that the π state rehybridizes with the σ state, leading to the $\pi+$ state, and then the linear energy dispersion peculiar to the Dirac electrons disappears in several cases associated with the opening of the energy gap. Moreover, we find that the substantial mixing of the $\pi+$ state, generated in such a way, with the states of the Ag atoms in the substrate converts the $\pi+$ state to the mixed $\pi+$ state and thus makes the state shift downwards or upwards, eventually annihilating Dirac electrons near the Fermi level. The absence of Dirac electrons caused in this way is found to be common to all the stable and metastable structures of the silicene on the Ag(111) substrates. We also find that the interaction between the $\pi+$ and the substrate orbitals should be weak enough to preserve Dirac electrons and at the same time be sizable to keep the system stable. We then propose two specific substrates as good candidates for the silicene with Dirac electrons, i.e., hexagonal BN and the hydrogen-processed Si(111) surface. We clarify that the silicene on those substrates are stable enough with the binding energy comparable to or twice that of the graphite and preserve Dirac electrons near the Fermi level.

DOI: 10.1103/PhysRevB.87.235435 PACS number(s): 73.22.−f, 68.43.Bc, 81.05.Zx

I. INTRODUCTION

Graphene is a hexagonally bonded carbon sheet in which sp^2 hybridized electrons (σ electrons) form a honeycomb structure and the remaining $\pi(p_z)$ electrons follow the massless Dirac (Weyl) equation. In the past decade, it has attracted great interest due to its intriguing properties.[1–6] The most outstanding property of graphene is the linear energy dispersion near the Fermi level (E_F) at particular symmetry points (Dirac cone), K and K', in the Brillouin zone (BZ).[7] This gives rise to unique phenomena such as the anomalous quantum Hall effect[1,2] and unexpected magnetic ordering.[8,9] Moreover, the very high in-plane mobility makes graphene a promising material utilized for next-generation devices.[10]

Inspired by the fruitful results obtained for graphene and in order to maximize the connectivity with semiconductor technology, the exploration for similar two-dimensional (2D) hexagonal materials of Si, which is located just below C in the periodic table, has been started. However, Si does not have any solid phase similar to graphite in nature, since the sp^3 hybridization of Si atoms is more favorable than the sp^2 hybridization. As a result, the hexagonal Si layer (silicene) is unable to be generated by exfoliation methods as performed in the case of graphene. An alternative way is to grow or synthesize silicene on substrates.[11–14] Recently, several experiments have indeed succeeded to synthesize silicene on Ag (Refs. 15–19) and on ZrB_2 (Ref. 20) surfaces, and the buckled silicene structures are identified by scanning tunneling microscopy (STM) measurements.

Theoretical investigations have been performed on the electronic properties of freestanding silicene.[21–24] It has been clarified by the local-density approximation (LDA) in the density-functional theory (DFT) that the freestanding silicene has a buckled honeycomb structure with the buckling of about a half angstrom and exhibits the graphenelike band structure around E_F, supporting the existence of charge carriers behaving as massless Dirac electrons.[22] The stronger spin-orbit interaction in Si than in C is also predicted to induce a detectable quantum spin Hall effect[23] and other attractive properties in silicene,[24–26] implying the great potential in future devices in nanoelectronics. However, in view of the compatibility with the current technology and also of the absence of solid-phase silicene as stated above, silicene should be synthesized and supported on suitable substrates. It is therefore extremely important to reveal the electronic structure in the real silicene on substrates.

Experimentally, the Si layer on the Ag(111) surface has been reported to exhibit several structures with the superperiodicity of 4×4,[15–17] $\sqrt{13} \times \sqrt{13}$,[16,17] $2\sqrt{3} \times 2\sqrt{3}$,[17,18,27] as well as $\sqrt{7} \times \sqrt{7}$ (Ref. 19) with respect to the 1×1 Ag(111) surface. Moreover, angular-resolved photoelectron spectroscopy (ARPES) measurements[15] suggest the existence of the linear energy dispersion near E_F in the 4×4 silicene/Ag(111) with a Fermi velocity (v_F) of 1.3×10^6 ms^{-1}. Another structure with the $\sqrt{3} \times \sqrt{3}$ periodicity with respect to the 1×1 silicene has been reported and the interference patterns observed by the scanning tunneling spectroscopy (STS) have been interpreted in terms of the linear energy dispersion near E_F with $v_F = 1.2 \times 10^6$ ms^{-1}.[28] The linear energy dispersion near E_F is believed to be the signature of the Dirac electrons in both experiments. However, the Fermi

velocities obtained in these experiments are two times larger than that of freestanding silicene[24] and even larger than that of graphene.[2]

On the other hand, no Landau-level sequences peculiar to the Dirac electrons have been observed in the STS measurements under the magnetic field performed for the 4×4 silicene/Ag(111).[29] It is also argued[29] that the linear energy dispersion observed in the ARPES experiment may be assigned to another band. It is thus highly desirable to clarify whether the Dirac electrons exist in silicene on Ag(111) surfaces through detailed first-principles calculations. Moreover it is of interest to explore possibilities of other substrates which may preserve the Dirac electrons in silicene.

In this paper, we report on extensive total-energy electronic-structure calculations in DFT for silicene on Ag(111) surfaces with the periodicities of 4×4, $\sqrt{13} \times \sqrt{13}$, and $2\sqrt{3} \times 2\sqrt{3}$ which are most commonly observed in the experiments. Several exchange-correlation energy functionals in DFT, i.e., LDA, the generalized gradient approximation (GGA) and the van der Waals functional, have been examined. An important finding common to all the stable and metastable structures that we have found is the disappearance of the Dirac electrons near E_F. With the combination of tight-binding (TB) calculations, we find that the buckling of the silicene layer and the strong mixing between Si and Ag orbitals are two important factors responsible for the disappearance of the Dirac electrons. We further clarify that the linear energy dispersion in the ARPES data corresponds to another band consisting of s and p orbitals of Ag substrate atoms. We finally propose on the basis of our DFT calculations that other substrates such as hexagonal boron nitride (h-BN) and the hydrogen-processed Si(111) surface are promising to preserve the Dirac electrons of silicene.

The rest of this paper is arranged as follows. In Sec. II we describe the methods of our calculations. In Sec. III, we show calculated results from our density-functional and tight-binding calculations performed for freestanding silicene in order to elucidate the difference from the silicene on substrates. In Sec. IV, we show the atomic structures, cohesive and binding energies, and the simulated STM images for the silicene/Ag(111) surfaces with various superperiodicities. In Sec. V, we present the electronic structures of the silicene on Ag(111) surfaces, discuss the disappearance of the Dirac electrons near E_F and the linear energy dispersions. In Sec. VI, we show the electronic structures of the silicene on h-BN and hydrogen-processed Si(111) substrates. Finally, we draw our conclusions in Sec. VII.

II. CALCULATION

The total-energy electronic-structure calculations have been performed in the density functional theory using either our real-space density-functional scheme (RSDFT code)[30,31] or the Vienna *ab initio* simulation package (VASP).[32,33] Most of the calculations have been done using LDA[34] and GGA[35] in our RSDFT, and the validity of the obtained results has been confirmed by comparing the main results with those from the van der Waals functional in DFT (vdW-DF).[36–38]

In the RSDFT calculations, the norm-conserving pseudopotentials are adopted[39] to describe the electron-ion interaction. The grid spacing in the RSDFT calculations is taken to be 0.16 Å corresponding to a cutoff energy of 108 Ry in the plane-wave basis-set calculations. Calculational parameters adopted here provide the lattice constant for the face-centered-cubic (fcc) Ag of 4.03 Å in LDA, 1.47% shorter than the experimental value (4.09 Å). In the VASP calculations, the electron-ion interaction is described by the projector augmented wave method,[40] and a plane-wave energy cutoff of 250 eV is used. The optB86b-vdW functional is adopted in vdW-DF calculations,[38] and the calculated lattice constant for the fcc Ag is 4.10 Å, 0.2% larger than the experimental value.

The silicene-covered Ag surface is simulated by a repeating slab model in which five-atomic-layer slabs are separated from each other by a 14-Å vacuum region. The geometry optimization is performed until the remaining forces become less than 26 meV/Å. The maximum spacing between the adjacent k points in the BZ integral is less than 0.05 $Å^{-1}$ in all the calculations.

In the TB calculation, we adopt a usual sp^3 model to consider the σ-π rehybridization in silicene. Although there have been sp^3 and sp^3s^* parameters reported for the freestanding silicene in other literature,[41,42] they are unable to represent the energy bands satisfactorily, in particular, the Dirac bands near E_F. Here we develop a set of first-nearest sp^3 parameters, by fitting the DFT results, which is capable of representing the energy bands of the freestanding silicene. The parameters we have determined are $E_s = -6.0$ eV, $E_p = -0.8$ eV, $V_{ss\sigma} = -2.2$ eV, $V_{sp\sigma} = 1.7$ eV, $V_{pp\sigma} = 2.3$ eV, and $V_{pp\pi} = -1.2$ eV. In order to consider the influence of the bond-length variation induced by the high buckling of the silicene layer on the Ag(111) surface, we adopt a correction method for the sp^3 parameters similar to that in Ref. 43, and the fitting parameters λ and the equilibrium lattice separation d_0 in the present work are set to be 2.0 and 2.24 Å, respectively.

III. FREESTANDING SILICENE

We have first examined structural and electronic properties of freestanding silicene. The lateral lattice constant, the buckling of the silicene plane (Δz), and the cohesive energy obtained by our LDA calculation are 3.82 Å, 0.43 Å, and 5.27 eV, respectively. The calculated energy bands of the freestanding 1×1 silicene are presented in Fig. 1(a), showing the Dirac cone at E_F. All these results are in good agreement with those reported by other groups.[22,24] The energy bands obtained by our TB model are shown in Fig. 1(b), which reproduce the LDA results satisfactorily, especially for the Dirac bands near E_F. This confirms the validity of our sp^3 TB parameters for the silicene structure.

Figure 1(c) shows calculated Kohn-Sham (KS) orbitals of the degenerate states at E_F of the geometry-optimized freestanding silicene. It is clearly shown that the states mainly consist of π and π^* orbitals. The small portion of σ orbitals is included due to the buckling, which is visible in Fig. 1(c). This π-σ rehybridization also manifests itself in our TB calculations. The degenerate states at E_F have characters of s, p_x, and p_y in our TB model, as opposed to the flat graphene: The amounts of those components are found to be as much as 1/3 of the p_z component, indicating the π-σ rehybridization. In spite of this rehybridization, the Dirac cone is still preserved

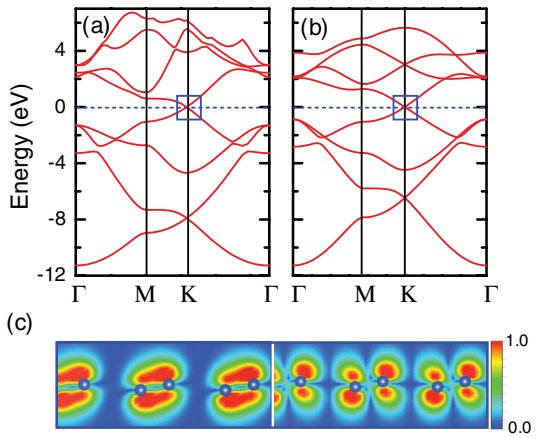

FIG. 1. (Color online) Calculated energy bands and Kohn-Sham (KS) orbitals of the stable low-buckled freestanding silicene. The energy bands are obtained (a) by the LDA calculations and (b) by our sp^3 TB calculations. E_F is shown by short-dashed lines. The KS orbitals of the π and π^* states which are rehybridized with σ and degenerate at E_F, indicated by the blue square in (a), are shown in (c). The contour values are normalized to the maximum.

due to the hexagonal symmetry of the geometry optimized silicene.

IV. ATOMIC STRUCTURES AND STM IMAGES OF SILICENE ON AG(111)

We have performed an extensive search for stable geometries of silicene/Ag(111). We notice that the 3×3 superperiodicity of silicene is commensurate to the 4×4 periodicity of Ag(111) with the lateral Si spacing of 2.23 Å, whereas the $\sqrt{7} \times \sqrt{7}$ periodicity of silicene is commensurate to the $\sqrt{13} \times \sqrt{13}$ and the $2\sqrt{3} \times 2\sqrt{3}$ periodicity of Ag(111) with the Si spacing of 2.28 and 2.19 Å, respectively. After extensive geometry optimization, we have reached two distinct structures for each of the 4×4, the $\sqrt{13} \times \sqrt{13}$, and the $2\sqrt{3} \times 2\sqrt{3}$ periodic silicene/Ag(111). The structural parameters of the obtained stable (S) and metastable (MS) geometries are shown in Table I. One of the characteristics common to all the S and MS structures is the complex and substantial buckling of the silicene: The surface-normal coordinate z of Si has 2–4 different values depending on the structures, as shown in Table I. The amount of the buckling is larger on average than that of the freestanding silicene. The average of the Si-Si distance $d_{\text{Si-Si}}$ is also larger than that of the freestanding silicene (2.24 Å in our calculation). It is of note that the average distance between silicene layer and Ag surface infers the formation of the chemical bonds in between.

TABLE I. Cohesive energy E_c (eV/Si atom) and the binding energy E_b (eV/Si atom) and the structural parameters calculated by LDA of the stable (S) and the metastable (MS) geometries for the silicene on the Ag(111) surfaces with the periodicities of 4×4, $\sqrt{13} \times \sqrt{13}$, and $2\sqrt{3} \times 2\sqrt{3}$. The $d_{\text{Si-Si}}$ (Å) is the average of the Si-Si distances (bond lengths) in silicene. The $d_{\text{si-Ag}}$ (Å) is the spacing between lowermost Si layer in the silicene (note: the silicene is buckled) and the topmost Ag layer. The Δz (Å) shows the Si coordinates in the surface-normal direction relative to that of the lowermost Si layer.

Periodicity	Str.	E_c	E_b	$d_{\text{Si-Si}}$	$d_{\text{si-Ag}}$	Δz
4×4	S	5.972	0.698	2.29	2.13	—,—, 0.78
	MS	5.968	0.694	2.29	2.11	0.57, 0.70, 0.90
$\sqrt{13} \times \sqrt{13}$	S	5.975	0.716	2.32	2.13	0.36, 0.59, 0.79
	MS	5.971	0.712	2.31	2.13	0.19, 0.52, 0.90
$2\sqrt{3} \times 2\sqrt{3}$	S	5.922	0.665	2.27	2.16	—, 0.36, 1.19
	MS	5.906	0.649	2.27	2.21	—,—,1.06

In order to clarify energetics of the silicene on the Ag(111) surface, we introduce two quantities, the cohesive energy E_c and the binding energy E_b which are defined as $E_c = (E_{\text{Ag(111)}} + N_{\text{Si}}\mu_{\text{Si}} - E_{\text{tot}})/N_{\text{Si}}$ and $E_b = (E_{\text{Ag(111)}} + E_{\text{silicene}} - E_{\text{tot}})/N_{\text{Si}}$, respectively. Here E_{tot}, $E_{\text{Ag(111)}}$, and E_{silicene} are the total energies of the silicene/Ag(111), the clean Ag(111) surface, and the freestanding silicene, respectively, N_{Si} is the number of Si atoms in the silicene, and μ_{Si} is the chemical potential of Si. As is clear from this definition, the binding energy is the energy gain per Si atom in the deposition of the silicene layer on the Ag(111) surface. When we use the total energy of an isolated Si atom for μ_{Si} in the definition of E_c, the cohesive energy means the energy gain to make the silicene on the Ag(111) from Si atoms. The calculated E_c and E_b are also shown in Table I.

Calculated cohesive energies for the stable and metastable structures for the $\sqrt{13} \times \sqrt{13}$ and the 4×4 surfaces are close to each other: E_c is the largest for the stable structure of the $\sqrt{13} \times \sqrt{13}$, followed by those for the other three structures with less than a 10-meV decrease. It is of note that E_c of the silicene is comparable with the cohesive energy of Si in diamond structure (6.02 eV in our LDA calculation), and larger than that of the freestanding silicene (5.27 eV in our LDA calculation), implying that Ag(111) surfaces are suitable stages to grow silicene. The adsorption energies for the $2\sqrt{3} \times 2\sqrt{3}$ surface is relatively smaller by 50–70 meV, reflecting the compression of the Si layer on this surface. The energetics obtained is consistent with that the $2\sqrt{3} \times 2\sqrt{3}$ surface is less frequently observed.[15–17,27,44] The calculated binding energies for the stable and the metastable structures are more than a half eV per Si atom which is substantially larger than the binding in graphite by an order of magnitude.[45] The calculated binding energies with more sophisticated exchange-correlation functionals will be discussed below.

The complex pattern of the buckling we have found leads to a rich variety of STM images. Figure 2 shows calculated STM images[46] of the stable and the metastable structures for the silicene/Ag with the 4×4, $\sqrt{13} \times \sqrt{13}$, and $2\sqrt{3} \times 2\sqrt{3}$ periodicities. The calculated STM image for the stable structure with each periodicity is in excellent agreement with the experiments.[15–18] Our stable structure for the 4×4 surface seems essentially identical to the structures proposed in the previous works.[15,16] The structures with other periodicities have been proposed[16,18] but the agreement with the experimental STM images is poor. On the contrary, the calculated STM images of our fully optimized structures reproduce characteristic features in the experiments: The moderately bright region of the lower half of the lateral cell in the $\sqrt{13} \times \sqrt{13}$ surface [Fig. 2(c)] and the superhexagonal structure in the $2\sqrt{3} \times 2\sqrt{3}$ surface [Fig. 2(e)]. This agreements show the importance of careful structural optimization.

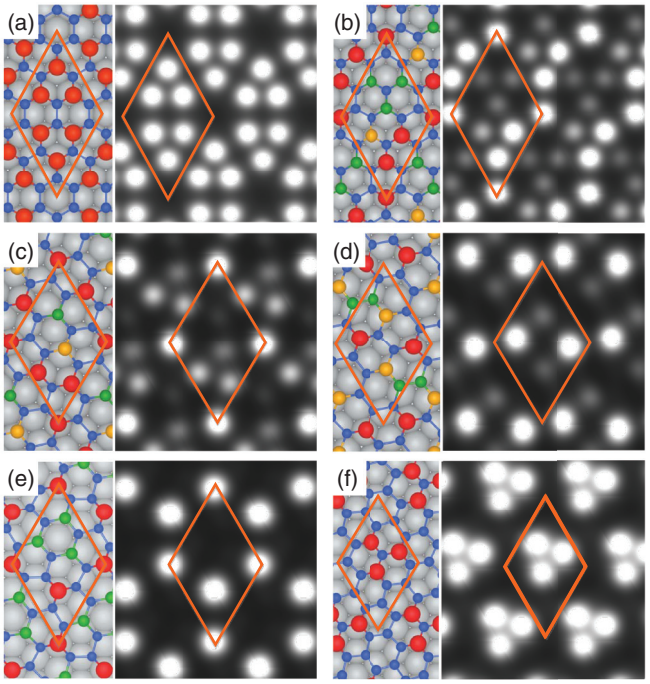

FIG. 2. (Color online) Calculated STM images (right parts) and top views of atomic structures (left parts) of the silicene on Ag(111) surfaces. The stable [(a), (c), and (e)] and the metastable [(b), (d), and (f)] structures with the 4×4 periodicity [(a) and (b)], the $\sqrt{13} \times \sqrt{13}$ periodicity [(c) and (d)], and the $2\sqrt{3} \times 2\sqrt{3}$ periodicity [(e) and (f)] are shown. Each circle of the left parts depicts the position of the Si atom in the silicene layer: The positions of the topmost Si and the bottommost Si are depicted by the largest (red) and the smallest (blue) circles; the intermediate-size circles depict the Si atoms between the top and the bottom. The large gray balls depict the positions of the substrate Ag atoms. The lateral unit cells are indicated by the orange lines.

The calculated cohesive energy of each structure corroborates the identification proposed here. The metastable structure with each periodicity exhibits the STM image different from that of the stable structure [Figs. 2(b), 2(d), and 2(f)], awaiting experimental observation.

It is known that LDA and vdW-DF provide substantial differences in atomic and electronic structures for graphene on metal surfaces in some cases.[47] We have thus performed calculations using the vdW-DF functional as well as GGA for the most important system, i.e., the stable structure of the 4×4 silicene/Ag(111).

We have found that the obtained stable structures are essentially identical in all the approximations (Table II). Considering that the atomic radii of Si and Ag are 1.18 and 1.65 Å, respectively, the bond lengths $d_{\text{Si-Ag}}$ shown in Table II clearly indicate the bond formation between silicene and the topmost Ag layer. The spacing between the lowermost silicene layer and the topmost Ag layer obtained in LDA is smaller than the corresponding value from vdW-DF by 2%, whereas that from GGA is larger than the vdW-DF value by about 1%. Also, the calculated binding energy is about a half eV per Si atom in all the approximations. This value is much larger than the typical van der Waals interaction energy manifested in the cases of graphene on metal surfaces,[47] and also of graphite

TABLE II. Structural parameters and binding energies for the stable structure of the 4×4 silicene/Ag(111) obtained by LDA, GGA (PBE), and vdW-DF calculations. The E_{b} (eV/Si atom), $d_{\text{si-Ag}}$ (Å) and $d_{\text{Si-Si}}$ (Å) are defined in the same way as that of Table I. The $d_{\text{Si-Ag}}$ (Å) is the distances (bond lengths) between Si and Ag atoms.

	$d_{\text{si-Ag}}$	$d_{\text{Si-Ag}}$	$d_{\text{Si-Si}}$	E_{b}
LDA (RSDFT)	2.13	2.56–2.81	2.29	0.698
GGA(RSDFT)	2.20	2.63–2.85	2.34	0.474
GGA (VASP)	2.18	2.65–2.88	2.33	0.453
vdW-DF (VASP)	2.17	2.62–2.90	2.33	0.652

as stated above, by an order of magnitude, indicating the covalent nature of the binding between the silicene and the Ag surface. Since the three approximations provide essentially identical results, we present the results from LDA below unless otherwise stated.

V. ABSENCE OF DIRAC ELECTRONS IN SILICENE ON AG(111)

A. Electronic structures of silicene on Ag(111)

We now discuss the electronic structures of the silicene on the Ag(111) surface. Figure 3 shows calculated energy bands of the stable structures of the 4×4 and the $\sqrt{13} \times \sqrt{13}$ silicene/Ag(111) surfaces. The K point in the BZ corresponding to the 1×1 silicene is folded on the Γ and the K in the 4×4 and the $\sqrt{13} \times \sqrt{13}$ surfaces, respectively. We have found no apparent energy bands near E_{F} which show linear energy dispersion peculiar to Dirac electrons. The energy bands of

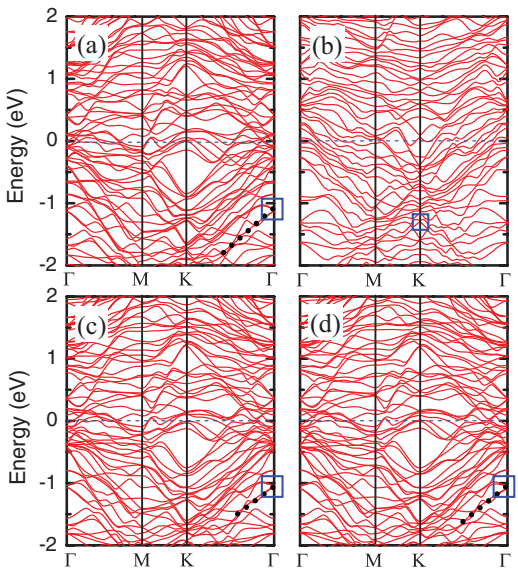

FIG. 3. (Color online) Calculated energy bands of the stable structures for the 4×4 (a) and the $\sqrt{13} \times \sqrt{13}$ (b) silicene/Ag(111) surfaces obtained by LDA. States marked by the square at either Γ or K in (a) and (b) have characters of mixed $\pi+$ and $\pi+^*$ as shown in Fig. 6 (see text). Energy bands of the stable structures for the 4×4 silicene/Ag(111) calculated by GGA and vdW-DF are also shown in (c) and (d), respectively. As marked by the black dots, it is clearly shown that one of the mixed $\pi+$ ($\pi+^*$) states for the 4×4 structure possesses the linear energy dispersion.

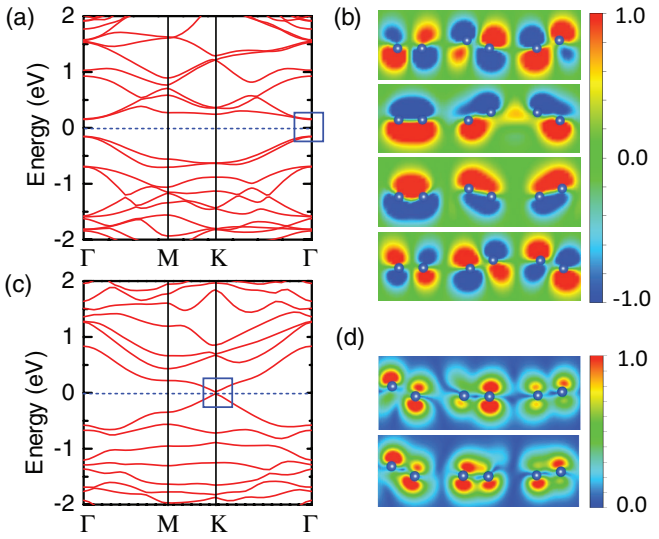

FIG. 4. (Color online) Calculated energy bands of the 3 × 3 silicene layer peeled from the stable 4 × 4 Ag surface (a) and the $\sqrt{7} \times \sqrt{7}$ silicene layer peeled from the stable $\sqrt{13} \times \sqrt{13}$ Ag surface (c). The contour plots of the KS orbitals of the 4 and 2 states near E_F marked by the squares in (a) and (c) are shown in (b) and (d), respectively.

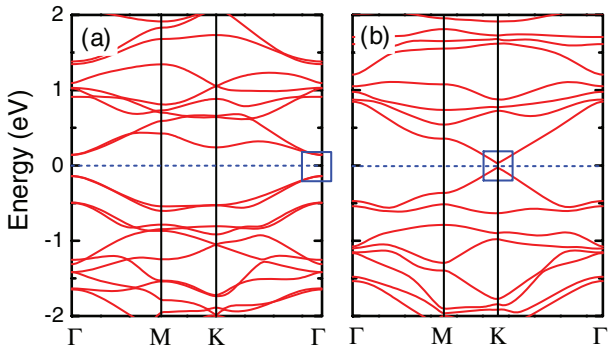

FIG. 5. (Color online) Energy bands of the 3 × 3 silicene layer peeled from the 4 × 4 Ag surface (a) and the $\sqrt{7} \times \sqrt{7}$ silicene layer peeled from the $\sqrt{13} \times \sqrt{13}$ Ag surface (b), obtained by our TB model. States marked by squares at the Γ and K point have characters of $\pi+$ and $\pi+^*$.

the silicene/Ag(111) with the 4 × 4 periodicity calculated by GGA and vdW-DF are also shown in Figs. 3(c) and 3(d). The calculated energy bands are similar to each other in all the three approximations.

In order to clarify underlying physics in the complex energy bands shown in Fig. 3, we then peel the silicene layer from the Ag substrate in the obtained stable silicene/Ag(111). The resultant peeled silicene exhibits the buckling, depending on the periodicity, as shown in the left parts of Figs. 2(a)–2(f). Figure 4 shows calculated energy bands of the freestanding 3 × 3 and $\sqrt{7} \times \sqrt{7}$ silicene layers which are peeled from the stable structures on the 4 × 4 and the $\sqrt{13} \times \sqrt{13}$ Ag surfaces, respectively.

We have found that four and two states, respectively, exist near E_F for the 3 × 3 [Fig. 4(a)] and $\sqrt{7} \times \sqrt{7}$ [Fig. 4(c)] peeled silicene. In the former case, there is a gap of 0.3 eV between the upper two and the lower two states, whereas in the latter case the two states are almost degenerate (with a small gap of 30 meV). The KS orbitals of these electron states near E_F are also shown in Fig. 4. In the geometry optimized freestanding silicene, the states are degenerate at E_F, showing the Dirac cone (Fig. 1). The character of the electron states are of π and π^* plus small σ. It is found that the KS orbitals of the peeled silicene keep the same character (Fig. 4). We thus call these states $\pi+$ and $\pi+^*$ states hereafter.

The $\pi+$ and $\pi+^*$ states in the peeled silicene show a recognizable difference from those in the structure-optimized freestanding silicene, however. In the peeled silicene, the way that the Si atoms are buckled is different from one to another. This indicates that the complex buckled geometries in the peeled silicene layers induce the complex π-σ rehybridization, which destroys the hexagonal symmetry and lifts a band gap in a certain case [Figs. 4(a) and 4(b)]. In particular, for the six top Si atoms of the 3 × 3 silicene layer [see Fig. 2(a) and Δz in Table I], the bond angles are about 109°, very close to the angle of ideally sp^3 hybridized Si atoms. The incorporation of sp^3-like hybridization by the high buckling corresponds to a large π-σ rehybridization in the silicene and thus induces a substantial energy gap. In the $\sqrt{7} \times \sqrt{7}$ silicene layer, the gap is very small presumably due to the less π-σ rehybridization related to the uneven arrangement of Si atoms with small Δz.

We have also performed the TB calculations using our sp^3 parameters. The calculated energy bands [Figs. 5(a) and 5(b)] are very similar to the RSDFT results [Figs. 4(a) and 4(c)]. By analyzing the eigenvectors of the $\pi+$ and the $\pi+^*$ states obtained from the TB calculations, we have indeed found that the p_z component is smaller in the 3 × 3 silicene layer than that in the $\sqrt{7} \times \sqrt{7}$ silicene layer. This confirms that the high buckling of the six top Si atoms induces the stronger π-σ rehybridization in the 3 × 3 silicene layer, which induces the larger band gap.

We now come back to the energy bands of the silicene on the Ag(111) substrate shown in Fig. 3. In the real silicene/Ag(111), it is found that the $\pi+$ and $\pi+^*$ states disappear near E_F. Detailed analyses of the KS orbitals clarify that the states which have the components of $\pi+$ or $\pi+^*$ orbitals exist in the valence bands. They are at 1.11 eV (1.28 eV) below E_F for the 4 × 4 ($\sqrt{13} \times \sqrt{13}$) surface (Fig. 3) at the Γ (K) point. Our calculation shows that the amount of the electron transfer from the Ag surface to the silicene is less than 0.43 (0.36) electron per unit cell for the 4 × 4 ($\sqrt{13} \times \sqrt{13}$) surface. This electron transfer causes the shift of E_F to the higher energy bands of the silicene by about a few tenths of eV, which is much smaller than the calculated shift of possible Dirac points.

Figures 6(a) and 6(b) show the KS orbitals of the above $\pi+$ and $\pi+^*$ states of the silicene on the Ag(111) substrate. It is found that those $\pi+$ and $\pi+^*$ states strongly mix with Ag orbitals at the top two layers of the substrate. This mixing leads to the formation of Si-Ag bonds in the stable structures, rendering the states deep in the valence bands. The antibonding counterparts indeed exist around 1 eV above E_F with the bonding-antibonding splitting being more than 2 eV. Dirac states, i.e., the $\pi+$ and $\pi+^*$ states, are converted to the mixed $\pi+$ and $\pi+^*$ states by the formation of chemical bonds between Si and Ag atoms, then shifted from E_F. We

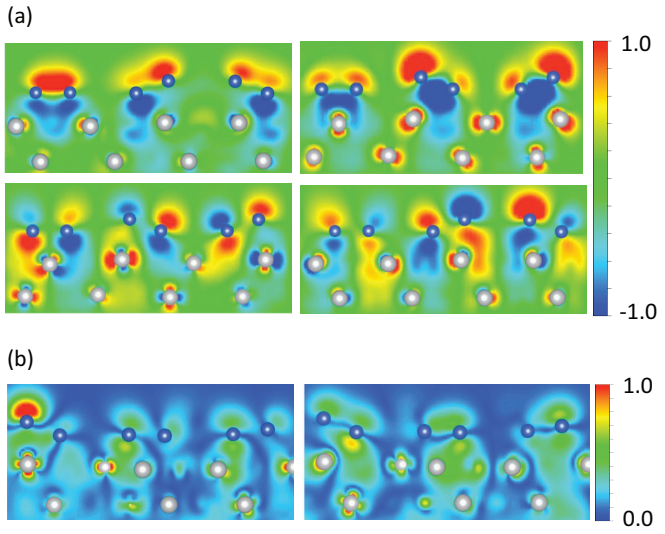

FIG. 6. (Color online) Contour plots of the KS orbitals of the mixed $\pi+$ ($\pi+^*$) states (see text) in the silicene/Ag(111) on the plane perpendicular to the silicene sheet. (a) The KS orbitals of the four mixed $\pi+$ ($\pi+^*$) states marked in Fig. 3(a) in the 4×4 silicene/Ag(111) at Γ point. (b) The KS orbitals of the two mixed $\pi+$ ($\pi+^*$) states marked in Fig. 3(b) in the $\sqrt{13} \times \sqrt{13}$ silicene/Ag(111) at K point. The blue and gray balls depict Si and Ag atoms, respectively.

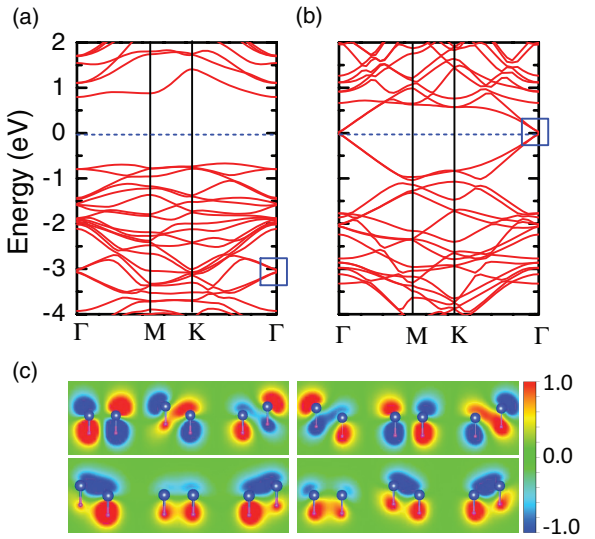

FIG. 7. (Color online) Calculated energy bands of the peeled 3×3 silicene with H atoms attached below the Si atoms (a) and of the same silicene but flattened and with the H atoms removed (b). The KS orbitals for the four mixed $\pi+$ ($\pi+^*$) states marked by the square at Γ in (a) are shown on the plane perpendicular to the silicene sheet in (c). These mixed states shift upward to E_F in (b) depicted as a square. The blue and pink balls depict Si and H atoms, respectively.

have confirmed that the absence of Dirac electrons found here is common to all the stable and metastable structures of the silicene on the Ag(111) substrate.

B. Absence of Dirac electrons in silicene

In the preceding subsection, we have found that the $\pi+$ and $\pi+^*$ states disappear near E_F in the silicene on the Ag(111) substrate whereas they remain near E_F in the peeled silicene. To further clarify the origin, we put hydrogen atoms below the peeled silicene with a fixed Si-H distance of 1.50 Å as substitutes for the Ag atoms. The energy bands and the KS orbitals of the resultant 3×3 silicene/H_{18} are shown in Figs. 7(a) and 7(c). We find that the mixed $\pi+$ ($\pi+^*$) states appear around -3.1 eV at Γ point but the degeneracy is lifted by 57 meV similar to that in the silicene on the Ag substrate [Fig. 3(a)]. The strong bonding between Si and H atoms renders the mixed $\pi+$ ($\pi+^*$) states far from E_F. Energy bands of the silicene peeled from the $\sqrt{13} \times \sqrt{13}$ Ag substrate with the H atoms attached show the essentially identical feature. We next make the 3×3 silicene/H_{18} flat and examine the band structures. The gap between the lifted mixed $\pi+$ ($\pi+^*$) states located at around -3.1 eV becomes 25 meV in this case, recovering almost the linear energy dispersion. This small gap of 25 meV is due to the lateral distortion of Si hexagons in the peeled silicene. We finally remove H atoms from the above flat 3×3 silicene/H_{18}. It is then found that the mixed $\pi+$ ($\pi+^*$) states lose the character of the hydrogen orbitals and shift upward at E_F with Dirac electrons being recovered, as is shown in Fig. 7(b).

We further consider a simple case: the planar bilayer silicene with AA stacking. In this case, the silicene has an ideal 2D hexagonal structure as graphene, and there is no charge transfer between the layers. Figure 8 shows the calculated energy bands and the KS orbitals of such bilayer silicene with an interlayer distance of 3.4 Å. Similar to the case of the silicene/Ag(111), the Dirac states (π and the π^* states in this case) are absent near E_F in the bilayer silicene. Instead, the π and π^* states in the two layers are mixed together, becoming the mixed π and π^* states. Then the bonding-character states appear around -1.1 eV at the K point, whereas the antibonding counterparts appear around 1.1 eV. We have also calculated the energy bands of the bilayer silicene with different interlayer distances, 4.0 and 5.6 Å, and found that the mixed bonding π (π^*) states appear around -0.6 eV and -0.1 eV at the K point, respectively. This shows that the shifts of the energy levels of the mixed π (π^*) states are proportional to the amount of the mixing between the orbitals, indicating that the Dirac electrons

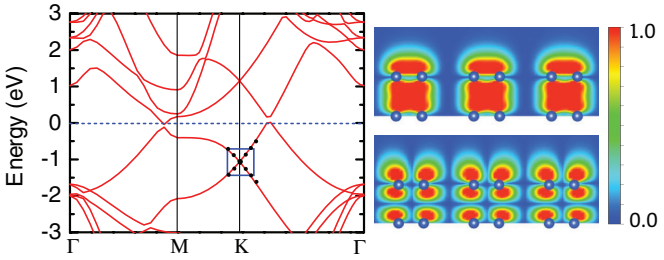

FIG. 8. (Color online) Calculated energy bands (left) and contour plots of the KS orbitals of the mixed π (π^*) states (right) of the AA stacked silicene bilayer with interlayer distance of 3.4 Å. The KS orbitals for the mixed π (π^*) states marked by the square are shown on the plane perpendicular to the silicene layer. As indicated by the black-dotted lines, the energy bands of the mixed π (π^*) states possess the linear energy dispersion near the K point.

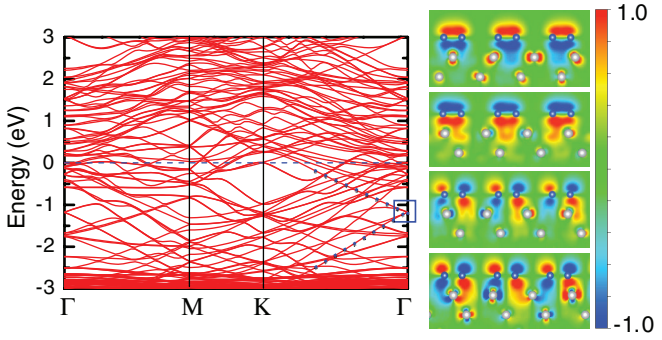

FIG. 9. (Color online) Calculated energy bands (left) and the contour plots of the KS orbitals of mixed π (π^*) states (right) for the ideally hexagonal planar 3×3 silicene on the 4×4 Ag surface. As marked by the blue-dotted lines, the energy bands of the mixed π (π^*) states possess the linear energy dispersion.

of silicene can be preserved only on the substrates with weak interaction.

Additionally, we show that the mixing with the substrate orbitals induces the disappearance of Dirac electrons near E_F even if the hexagonal symmetry of silicene is well preserved. Here we consider the ideally hexagonal planar 3×3 silicene on the 4×4 Ag substrate. The distance between the silicene and the Ag surface is fixed to be 2.4 Å, which is the average distance between the silicene layer and the Ag surface in the stable silicene on the Ag(111) [Fig. 2(a) and Table I]. The calculated energy bands are shown in Fig. 9, where the Dirac π (π^*) states indeed disappear near E_F. Instead, the mixed π (π^*) states (the right panel of Fig. 9) appear around 1.2 eV below E_F, the location of which is very similar to that of the buckled stable silicene on the Ag(111) as in Fig. 3(a).

We now recognize that two factors are important in the disappearance of Dirac electrons in silicene: the buckling of the silicene layer and the mixing with the substrate orbitals. Our calculations show that the buckling or the corrugation of Si atoms in the silicene induces the rehybridization of the π and π^* orbitals with the σ orbital, leading to the $\pi+$ and the $\pi+^*$ states. This buckling is usually associated with the breaking of the hexagonal symmetry, thus leading to the disappearance of the linear energy dispersion and the lifting of the degeneracy. When the silicene stands alone, no matter how the rehybridization between the π and the σ takes place, the $\pi+$ and $\pi+^*$ states stay near E_F. Then when the silicene is placed on the substrate, the strong mixing with the substrate orbitals induces the mixed states which are shifted downwards, being located deep in the valence bands.

C. Linear energy dispersion of the mixed $\pi+$ and $\pi+^*$ states

The linear energy dispersion is regarded as one of the characteristics of the Dirac states. We have indeed found that the $\pi+$ and the $\pi+^*$ states show the linear energy dispersion as long as the π-σ rehybridization is weak enough [Figs. 1, 7(b), 8, and 9]. It is noteworthy that the mixing of the $\pi+$ and the $\pi+^*$ states with the substrate Ag orbitals also affects the destruction and the preservation of the linear energy dispersion. The positions of surface Ag atoms relative to a Si atom in the silicene depend on the position of the Si atom, and thus the amount of the mixing of each $\pi+$ ($\pi+^*$) with the Ag orbitals depends on the Si-atom site. This causes inequivalence among the Si-atom sites and thus symmetry lowering, and then reduces the linearity of the energy dispersion (a negative effect). On the other hand, the strong mixing with the substrate orbitals occasionally increases the component of p_z orbitals in the $\pi+$ state of the silicene and effectively reduces the π-σ rehybridization. As a result, the linear energy dispersion may be recovered (a positive effect). Therefore, competing mechanisms exist for the linearity of the energy dispersion of the mixed $\pi+$ ($\pi+^*$) states.

For the stable structure of the $\sqrt{13} \times \sqrt{13}$ silicene/Ag(111), the π-σ rehybridization is minor and the peeled silicene show rather linear energy dispersion [Fig. 4(c)]. Yet the silicene has a complex buckling geometry as is shown in Fig. 2(c). This makes the negative effect of the substrate-$\pi+$ mixing dominant, and thus the linear energy dispersion is broken [Fig. 3(b)]. As for the stable structure of the 4×4 silicene/Ag(111), the π-σ rehybridization is prominent, as is shown in the peeled silicene [Fig. 4(a)]. Yet the buckling geometry of silicene is simpler and still keeps some hexagonal symmetry [Fig. 2(a)]. In this case, the positive effect of the substrate-$\pi+$ mixing holds and the hexagonal symmetry is effectively and partially recovered. As a result, the linear energy dispersion is preserved as in Fig. 3(a). The above results show that the linear energy dispersion is not a direct evidence of Dirac electrons.

D. Linear energy in the ARPES experiment

Although one of the mixed $\pi+$ and $\pi+^*$ states of the stable structure of the 4×4 silicene/Ag(111) exhibits the linear energy dispersion, it is obviously different from that observed by the ARPES experiment, which appears near E_F with a much larger Fermi velocity $v_F = \hbar^{-1} d\varepsilon/dk$.[15] The linear energy dispersion in the experiment appears in the energy range of $[-0.3, -3.0]$ in units of eV which corresponds to the wave number length $\Delta k \approx 0.35$ Å^{-1} along the K-Γ line in the BZ of 1×1 silicene [i.e., the Γ-K line in the BZ of the 4×4 silicene/Ag(111)]. By examining the calculated energy bands of the 4×4 silicene/Ag(111), we have indeed found a quasilinear energy dispersion which corresponds to the ARPES experiment. Figure 10(a) shows the enlargement of the energy bands for the stable structure of the 4×4 silicene/Ag(111). We observe the quasilinear energy dispersion along the Γ-K line. We have then analyzed the characters of the energy band which show the quasilinear energy dispersion. Figure 11(a) shows the KS orbital at a BZ point marked by the square in Fig. 10(a) of the quasilinear energy band. It is found that the KS orbital is distributed mainly on the Ag atoms with the characters of s and p orbitals. The energy band which shows the quasilinear dispersion is thus identified as the sp band of the Ag surface.

To corroborate this character, we have also calculated the energy bands of the clean Ag(111) surface with the 4×4 periodicity [Fig. 10(b)]. We have obtained the quasilinear energy band also on the clean Ag(111) surface. The corresponding KS orbital on the clean Ag(111), shown in Fig. 11(b), is essentially identical to the KS orbital in the silicene/Ag(111) [Fig. 11(a)]. Hence it is highly likely that the ARPES experiment has

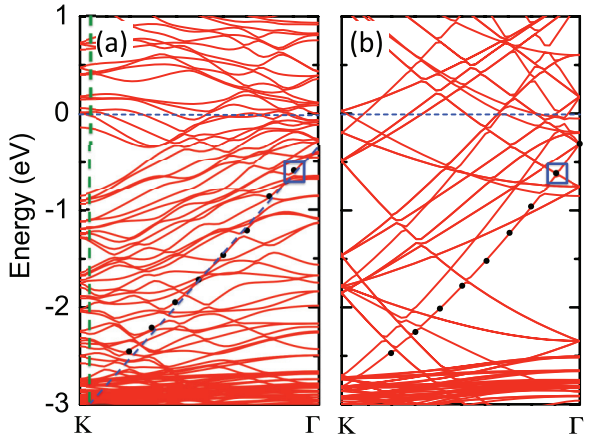

FIG. 10. (Color online) Calculated energy bands for the stable structure of the 4×4 silicene/Ag(111) (a) and for the clean Ag(111) surface with the 4×4 periodicity (b). The green-dashed line corresponds to the BZ position where the energy of the linear band (indicated by the blue-dashed line) in the ARPES experiment (Ref. 15) reaches -3.0 eV. The sequence of the states marked by the black dots shows the quasilinear energy dispersion.

detected the Ag(111) surface energy bands which are sensitive to the photoemission processes. This conclusion is supported by another recent study.[29]

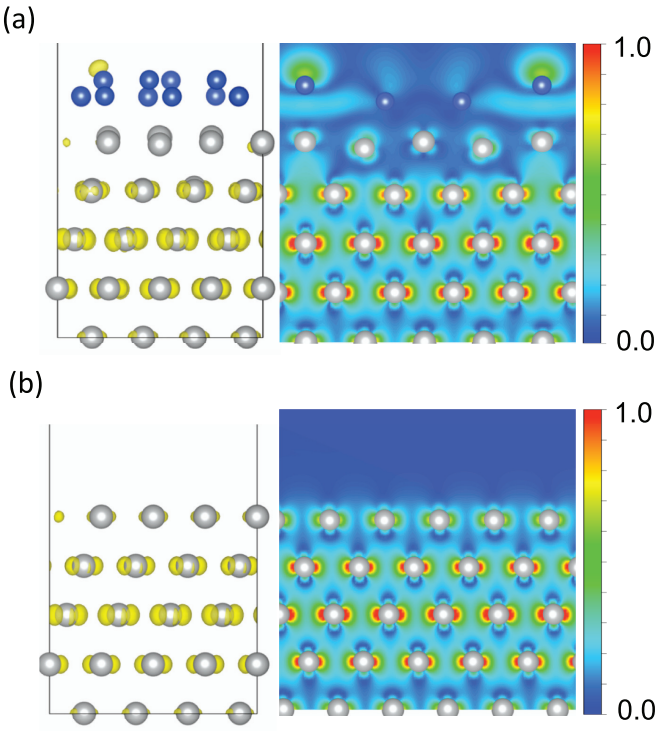

FIG. 11. (Color online) KS orbitals of the quasilinear energy bands for the stable structure of the 4×4 silicene/Ag(111) (a) and of the clean Ag(111) surface with the 4×4 periodicity (b). The KS orbitals corresponding to the states marked by the blue squares in Fig. 10 are shown. Left: Isovalue surface viewed along the $[01\bar{1}]$ direction at its value of 33% of the maximum value. Right: The contour plot of the KS orbital on $(1\bar{1}1)$ plane. The blue and gray balls depict Si and Ag atoms, respectively.

VI. SILICENE ON BN AND H-PROCESSED SI(111) SUBSTRATES

Our calculations for the silicene on the Ag surface presented above has unequivocally clarified that the hexagonal symmetry with less buckling is the principal factor to preserve Dirac electrons and then the weak silicene-substrate interaction is crucial to keep them near E_F. Based on this knowledge, we here propose that the hexagonal BN and the hydrogen-processed Si(111) surface are good candidates to preserve Dirac electrons in silicene.

As the first candidate for the substrate, we consider the h-BN with the AA' stacking.[48,49] We notice that the silicene with the $\sqrt{3} \times \sqrt{3}$ periodicity is commensurate with $\sqrt{7} \times \sqrt{7}$ supercell of h-BN with the lattice mismatch of 0.64%. We have considered four representative arrangements of silicene on h-BN, where a Si atom is located on either a B atom, a N atom, the center of a B-N bond (bridge), or the center of the BN hexagonal ring (hollow). We have found that the bridge configuration (inset of Fig. 12) is the most stable, although the energy differences among different configurations are very small (1 meV per Si atom at most). The calculated binding energy for the bridge configuration between silicene and h-BN is 56 meV per Si atom with the optimized interlayer distance of 3.23 Å (similar to the evaluated distance in a h-BN/silicene/h-BN structure[25]). This value is comparable with the binding energy of graphite. The calculated energy bands and the KS orbitals are shown in Fig. 12, where the mixed $\pi+(\pi+^*)$ states indeed appear at E_F with the tiny gap of 10 meV and with the linear energy dispersion characteristic to Dirac electrons.

Figure 13 shows the calculated energy bands and the KS orbitals of the silicene on the hydrogen-monolayer-covered Si(111) surface. The passivation of Si surfaces with the hydrogen monolayer is very common in processing specimens in semiconductor science and technology. The deposition of a Si monolayer, i.e., the silicene, on the H-covered Si surface is likely to be achieved, although the substitution of the H atoms by the top-layer Si atoms takes place at the initial stage

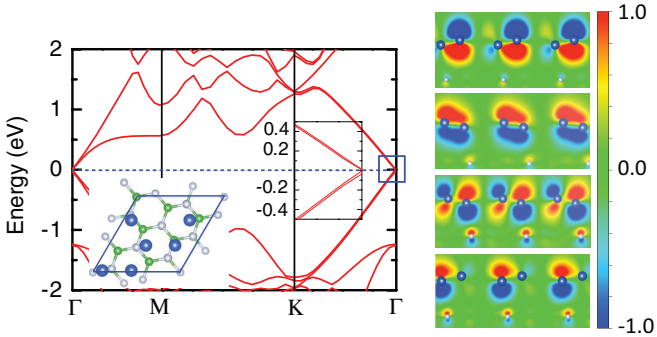

FIG. 12. (Color online) Calculated energy bands and contour plots of the mixed $\pi+(\pi+^*)$ states at Γ point of the silicene on h-BN with the bridge configuration. Enlarged energy bands near $E_F = 0$ are shown in the inset. The KS orbitals of the mixed $\pi+(\pi+^*)$ states marked by the square are shown on the plane perpendicular to the silicene layer in the right panel. The top view of the optimized structure is shown in the inset of the left panel, where the lateral unit cell is indicated by the blue lines and the blue, green, and gray balls depict the Si atoms, B atoms, and N atoms, respectively.

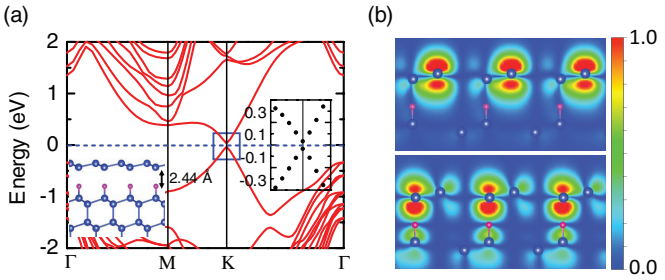

FIG. 13. (Color online) Calculated energy bands (a) of the silicene on the hydrogen-covered Si(111) surface [inset of (a)] and contour plots of the mixed $\pi+$ ($\pi+^*$) states (b). Enlarged energy bands near $E_F = 0$ are shown in another inset and the distributions of the mixed $\pi+$ ($\pi+^*$) states at K point marked by the square are shown on the plane perpendicular to the surface. The blue and pink balls in the inset depict Si and H atoms, respectively.

of the Si deposition.[50,51] Alternatively, the H insertion in the subsurface is used to cut Si crystal[52] and the single-layer H insertion may be possible in the future. We have indeed found that the silicene on the H-covered Si(111) surface is stable with the separation between the top Si layer and the H layer of 2.44 Å (inset of Fig. 13). The calculated binding energy of the top Si layer to the H-covered Si(111) surface is 140 meV per Si atom. It is found that the top Si layer keeps the hexagonal structure with the variation in the surface-normal coordinate of $\Delta z = 0.48$ Å. The energy bands and the KS orbitals clearly show the existence of Dirac electrons at E_F.

To examine the stability of the above two structures, we have set the initial spacing between the silicene layer and the h-BN or the H layer to be as small as 1.5 Å, where the silicene layer may chemically interact with the substrates. After geometry optimization, however, the separation of the silicene-BN and the silicene-H layers recovers to 3.23 and 2.44 Å, respectively, indicating that the silicene is stable on two such substrates with weak interactions. We have further examined the effect of van der Waals interactions by using vdW-DF calculations. It is found that the separation of silicene-BN and silicene-H layers are 3.39 and 2.61 Å, respectively, and the binding energies are comparable with those by LDA, showing that the structures are stable. The corresponding energy bands are also very similar with the LDA results, with the Dirac electrons appearing at E_F.

VII. CONCLUSION

We have performed the total-energy electronic-structure calculations on the basis of the density-functional theory for the silicene on several substrates as well as the freestanding silicene. On the Ag(111) surfaces which are most commonly used as substrates for the silicene in current experiments, we have found that the silicene is buckled substantially so that the π state rehybridizes with the σ state, leading to the $\pi+$ state, and then the linear energy dispersion peculiar to the Dirac electrons disappears in several cases associated with the opening of the energy gap. Moreover, we have found that the substantial mixing of the $\pi+$ state, generated in such a way, with the states of the Ag atoms in the substrate converts the $\pi+$ state to the mixed $\pi+$ state and thus makes the state shift downwards or upwards, eventually annihilating Dirac electrons near the Fermi level. The absence of Dirac electrons caused in this way is found to be common to all the stable and metastable structures of the silicene on the Ag(111) substrates which are either experimentally identified or theoretically predicted in this work, including the 4×4, $\sqrt{13} \times \sqrt{13}$, and $2\sqrt{3} \times 2\sqrt{3}$ periodic structures. The several distinct structures which we have determined in our calculations show the excellent agreement with the scanning tunneling microscopy measurement in their structural characteristics. The metastable structures which we have found have very comparable total energies within 10 meV per Si atom compared with the most stable structures, awaiting experimental observations. Based on the results of the detailed calculations for the silicene on the Ag(111) substrate, we have found that the interaction between the $\pi+$ and the substrate orbitals should be weak enough to preserve Dirac electrons and at the same time be sizable to keep the system stable. We have then proposed two specific substrates as good candidates for the silicene with Dirac electrons: i.e., hexagonal BN and the hydrogen-processed Si(111) surface. Detailed density-functional calculations clearly revealed that the silicene on the h-BN and the silicene on the H-covered Si(111) substrate are stable enough with the binding energy comparable to or twice that of the graphite and with Dirac electrons beautifully preserved near the Fermi level.

We have also developed a tight-binding model and analyzed the DFT results in this paper. This model may be useful to explore the properties of the silicene in future.

ACKNOWLEDGMENTS

This work was supported by the research project "Materials Desighn through Computics" (http://computics-material.jp/index-e.html) by MEXT and also by "Computational Materilas Science Initiative" by MEXT, Japan. Computations were performed mainly at Supercomputer Center in ISSP, University of Tokyo. Z.X. acknowledges the support of NSFC (Grant No. 11204259).

*On leave from Xiangtan University, Xiangtan, Hunan 411105, China.

[1] K. S. Novoselov, A. K. Geim, S. V. Morozov, D. Jiang, M. L. Katsnelson, I. V. Grigorieva, S. V. Dubonos, and A. A. Firsov, Nature (London) **438**, 197 (2005).

[2] Y. Zhang, Y.-W. Tan, H. L. Stormer, and P. Kim, Nature (London) **438**, 201 (2005).

[3] A. K. Geim, Science **324**, 1530 (2009).

[4] A. A. Balandin, S. Ghosh, W. Bao, I. Calizo, D. Teweldebrhan, F. Miao, and C. N. Lau, Nano Lett. **8**, 902 (2008).

[5] Z. X. Guo, D. Zhang, and X. G. Gong, Appl. Phys. Lett. **95**, 163103 (2009).

[6]Z. X. Guo, J. W. Ding, and X. G. Gong, Phys. Rev. B **85**, 235429 (2012).
[7]J. C. Slonczewski and P. R. Weiss, Phys. Rev. **109**, 272 (1958).
[8]Y. W. Son, M. L. Cohen, and S. G. Louie, Nature (London) **444**, 347 (2007).
[9]S. Okada and A. Oshiyama, Phys. Rev. Lett. **87**, 146803 (2001).
[10]International Technology Roadmap for Semiconductors, http://www.itrs.net/.
[11]P. De Padova, C. Quaresima, C. Ottaviani, P. M. Sheverdyaeva, P. Moras, C. Carbone, D. Topwai, B. Olivieri, A. Kara, H. Oughaddou, B. Aufray, and G. Le Lay, Appl. Phys. Lett. **96**, 261905 (2010).
[12]P. De Padova, C. Quaresima, B. Olivieri, P. Perfetti, and G. Le Lay, Appl. Phys. Lett. **98**, 081909 (2011).
[13]G. Le Lay, B. Aufray, C. Landri, H. Oughaddou, J. P. Biberian, P. De Padova, M. E. Dvila, B. Ealet, and A. Kara, Appl. Surf. Sci. **256**, 524 (2009).
[14]A. Kara, H. Enriquez, A. P. Seitsonen, L. C. Lew, Yan Voon, S. Vizzini, B. Aufray, and H. Oughaddou, Surf. Sci. Rep. **67**, 1 (2012).
[15]P. Vogt, P. De Padova, C. Quaresima, J. Avila, E. Frantzeskakis, M. C. Asensio, A. Resta, B. Ealet, and G. Le Lay, Phys. Rev. Lett. **108**, 155501 (2012).
[16]C. L. Lin, R. Arafune, K. Kawahara, N. Tsukahara, E. Minamitani, Y. Kim, N. Takagi, and M. Kawai, Appl. Phys. Exp. **5**, 045802 (2012).
[17]H. Jamgotchian, Y. Colington, N. hamzaouri, B. Ealet, J. Hoarau, B. Aufray, and J. P. Bibérian, J. Phys.: Condens. Matter **24**, 172001 (2012).
[18]B. Feng, Z. Ding, S. Meng, Y. Yao, X. He, P. Cheng, L. Chen, and K. Wu, Nano Lett. **12**, 3507 (2012).
[19]D. Chiappe, C. Grazianetti, G. Tallarida, M. Fanciulli, and A. Molle, Adv. Mater. **24**, 5088 (2012).
[20]A. Fleurence, R. Friedlein, T. Ozaki, H. Kawai, Y. Wang, and Y. Yamada-Takamura, Phys. Rev. Lett. **108**, 245501 (2012).
[21]K. Takeda and K. Shiraishi, Phys. Rev. B **50**, 14916 (1994).
[22]S. Cahangirov, M. Topsakal, E. Aktürk, H. Sąhin, and S. Ciraci, Phys. Rev. Lett. **102**, 236804 (2009).
[23]C. C. Liu, W. Feng, and Y. Yao, Phys. Rev. Lett. **107**, 076802 (2011).
[24]N. D. Drummond, V. Zólyomi, and V. I. Fal'ko, Phys. Rev. B **85**, 075423 (2012).
[25]Z. Ni, Q. Liu, K. Tang, J. Zheng, J. Zhou, R. Qin, Z. Gao, D. Yu, and J. Lu, Nano Lett. **12**, 113 (2012).
[26]L. Pan, H. J. Liu, X. J. Tan, H. Y. Lv, J. Shi, X. F. Tang, and G. Zheng, Phys. Chem. Chem. Phys. **14**, 13588 (2012).
[27]B. Lalmi, H. Oughaddou, H. Enriquz, A. Kara, S. Vizzini, B. Eaqlet, and B. Aufray, Appl. Phys. Lett. **97**, 223109 (2010) the reported Si-Si separation of 1.9 Å therein is questionably small.
[28]L. Chen, C. C. Liu, B. Feng, X. He, P. Cheng, Z. Ding, S. Meng, Y. Yao, and K. Wu, Phys. Rev. Lett. **109**, 056804 (2012).
[29]C. L. Lin, R. Arafune, K. Kawahara, M. Kanno, N. Tsukahara, E. Minamitani, Y. Kim, M. Kawai, and N. Takagi, Phys. Rev. Lett. **110**, 076801 (2013).
[30]J. I. Iwata, D. Takahashi, A. Oshiyama, B. Boku, K. Shiraishi, S. Okada, and K. Yabana, J. Comput. Phys. **229**, 2339 (2010).
[31]Y. Hasegawa, J.-I. Iwata, M. Tsuji, D. Takahashi, A. Oshiyama, K. Minami, T. Boku, F. Shoji, A. Uno, M. Kurokawa, H. Inoue, I. Miyoshi, and M. Yokokawa, *Proceedings of the 2011 International Conference on High Performance Computing, Networking, and Storage Analysis*, ACM Digital Library, article no 1 (Association of Computing Machinery, http://dl.acm.org/).
[32]G. Kresse and J. Hafner, Phys. Rev. B **49**, 14251 (1994).
[33]G. Kresse and J. Furthmuller, Phys. Rev. B **54**, 11169 (1996).
[34]J. P. Perdew and A. Zunger, Phys. Rev. B **23**, 5048 (1981).
[35]J. P. Perdew, K. Burke, and M. Ernzerhof, Phys. Rev. Lett. **77**, 3865 (1996).
[36]M. Dion, H. Rydberg, E. Schröder, D. C. Langreth, and B. I. Lundqvist, Phys. Rev. Lett. **92**, 246401 (2004).
[37]T. Thonhauser, V. R. Cooper, S. Li, A. Puzder, P. Hyldgaard, and D. C. Langreth, Phys. Rev. B **76**, 125112 (2007).
[38]J. Klimeš, D. R. Bowler, and A. Michaelides, Phys. Rev. B **83**, 195131 (2011).
[39]N. Troullier and J. L. Martins, Phys. Rev. B **43**, 1993 (1991).
[40]G. Kresse and D. Joubert, Phys. Rev. B **59**, 1758 (1999).
[41]G. G. Guzmán-Verri and L. C. Lew Yan Voon, Phys. Rev. B **76**, 075131 (2007).
[42]C. C. Liu, H. Jiang, and Y. Yao, Phys. Rev. B **84**, 195430 (2011).
[43]J. W. Ding, X. H. Yan, J. X. Cao, D. L. Wang, Y. Tang, and Q. B. Yang, J. Phys.: Condens. Matter **15**, L439 (2003).
[44]G. L. Lay, P. D. Padova, A. Resta, T. Bruhn, and P. Vogt, J. Phys. D: Appl. Phys. **45**, 392001 (2012).
[45]I. Hamada and M. Otani, Phys. Rev. B **82**, 153412 (2010), and references therein.
[46]STM images are calculated by the scheme developed in J. Tersoff and D. R. Hamann, Phys. Rev. B **31**, 805 (1985).
[47]M. Vanin, J. J. Mortensen, A. K. Kelkkanen, J. M. Garcia-Lastra, K. S. Thygesen, and K. W. Jacobsen, Phys. Rev. B **81**, 081408 (2010).
[48]J. E. Padilha, R. B. Pontes, and A. Fazzio, J. Phys.: Condens. Matter **24**, 075301 (2012).
[49]J. H. Warner, M. H. Rummeli, A. Bachmatiuk, and B. Buchner, ACS Nano **4**, 1299 (2010).
[50]S. Jeong, Surf. Sci. **530**, 155 (2003).
[51]S. Jeong and A. Oshiyama, Phys. Rev. Lett. **79**, 4425 (1997); Phys. Rev. B **58**, 12958 (1998).
[52]M. Bruel, Electron. Lett. **31**, 1201 (1995); K. V. Srikrishnan, US Patent No. 5,882,987 (Smart-Cut) (March, 1999).